H1prelim-08-041 Submitted to

XVI International Workshop on Deep-Inelastic Scattering, DIS2008, April 7-11, 2008, London
Parallel Session **Structure Functions**

Electronic Access:https://www-h1.desy.de/publications/H1preliminary.short_list.html

A Measurement of the Longitudinal Proton Structure Function $F_L(x, Q^2)$ at low x and medium Q^2 in the H1 Experiment at HERA

H1 Collaboration

Abstract

A measurement of the longitudinal proton structure function $F_L(x, Q^2)$ derived from inclusive deep inelastic ep scattering cross section measurements with the H1 detector at HERA is presented. The data were taken in the year 2007 at a positron beam energy of $E_e = 27.5$ GeV and proton beam energies E_p of 920 GeV, 575 GeV and 460 GeV. The cross section measurement is performed in a range of medium four-momentum transfer squared $12 \leq Q^2 \leq 90$ GeV^2 and correspondingly low Bjorken-x between $0.00024 \leq x \leq 0.00362$. The measured longitudinal structure function is found to be consistent with the NLO QCD calculations based on H1PDF fit and MSTW.

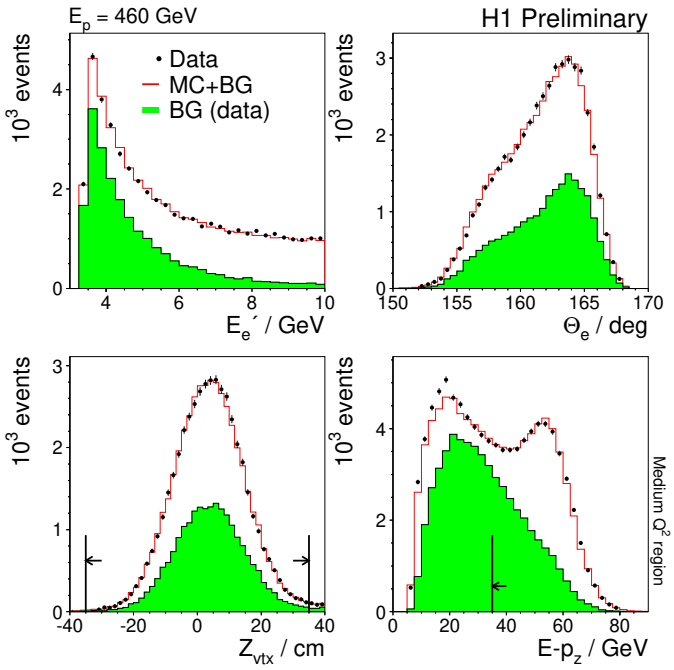

Figure 1: Comparison of the correct charge sign data (points) with a sum of background determined from the wrong charge sign data (green histogram) and DIS MC (open histogram) for the low proton beam energy (460 GeV). The distributions from the left to the right and from the top to the bottom are the scattered electron energy $E_e^{'}$, the scattered electron polar angle Θ_e, the z-position of the event vertex Z_{vtx} and the sum $E - p_z$ of all final state particles. The vertical lines in Z_{vtx} and $E - p_z$ distributions indicate cut values.

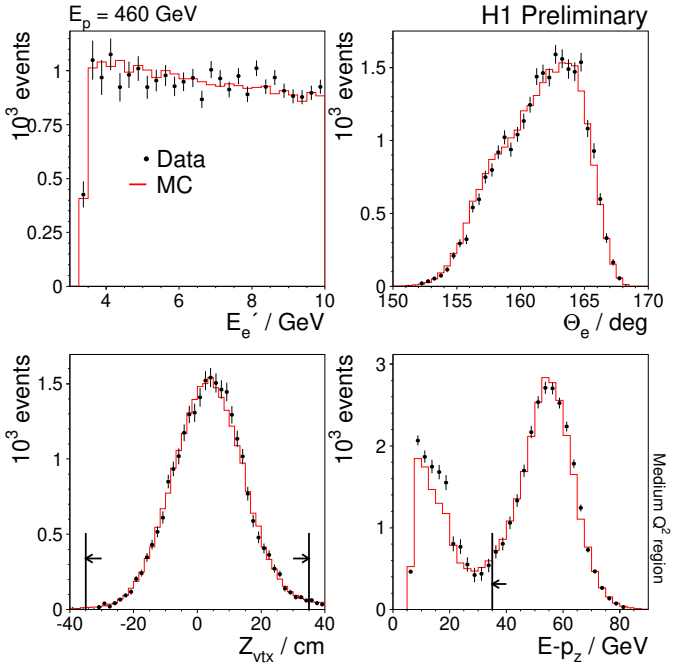

Figure 2: Comparison of signal distributions (background subtracted with corresponding asymmetry factor) for the low proton beam energy (460 GeV). The distributions from the left to the right and from the top to the bottom are the scattered electron energy $E_e^{'}$, the scattered electron polar angle Θ_e, the z-position of the event vertex Z_{vtx} and the sum $E - p_z$ of all final state particles. The vertical lines in Z_{vtx} and $E - p_z$ distributions indicate cut values.

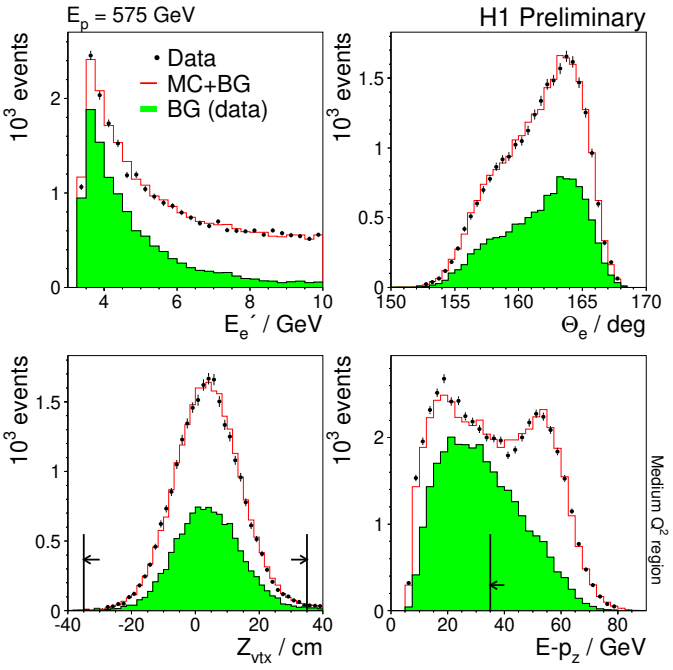

Figure 3: Comparison of the correct charge sign data (points) with a sum of background determined from the wrong charge sign data (green histogram) and DIS MC (open histogram) for the medium proton beam energy (575 GeV). The distributions from the left to the right and from the top to the bottom are the scattered electron energy $E_e^{'}$, the scattered electron polar angle Θ_e, the z-position of the event vertex Z_{vtx} and the sum $E-p_z$ of all final state particles. The vertical lines in Z_{vtx} and $E-p_z$ distributions indicate cut values.

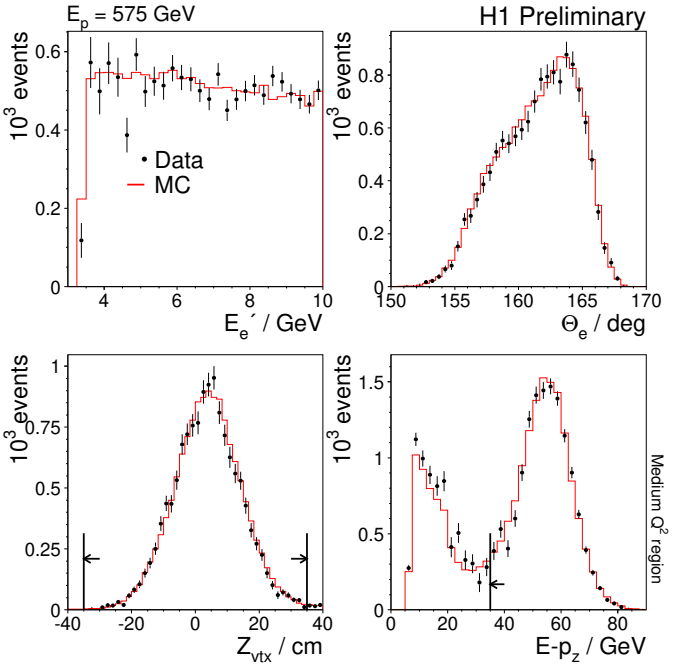

Figure 4: Comparison of signal distributions (background subtracted with corresponding asymmetry factor) for the medium proton beam energy (575 GeV). The distributions from the left to the right and from the top to the bottom are the scattered electron energy $E_e^{'}$, the scattered electron polar angle Θ_e, the z-position of the event vertex Z_{vtx} and the sum $E-pz$ of all final state particles. The vertical lines in Z_{vtx} and $E-p_z$ distributions indicate cut values.

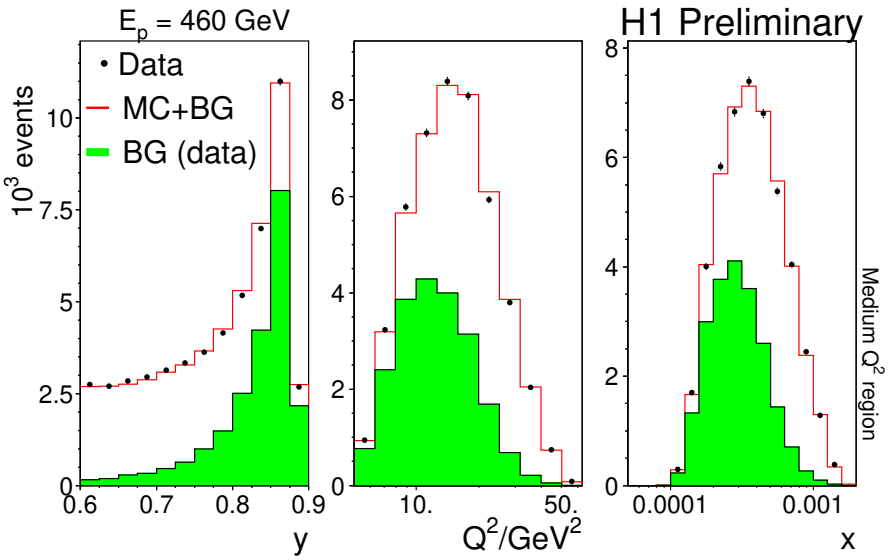

Figure 5: Comparison of the correct charge sign data (points) with a sum of background determined from the wrong charge sign data (green histogram) and DIS MC (open histogram) for the low proton beam energy (460 GeV). The distributions from the left to the right are the inelasticity y, the four-momentum transfer squared Q^2 and Bjorken x.

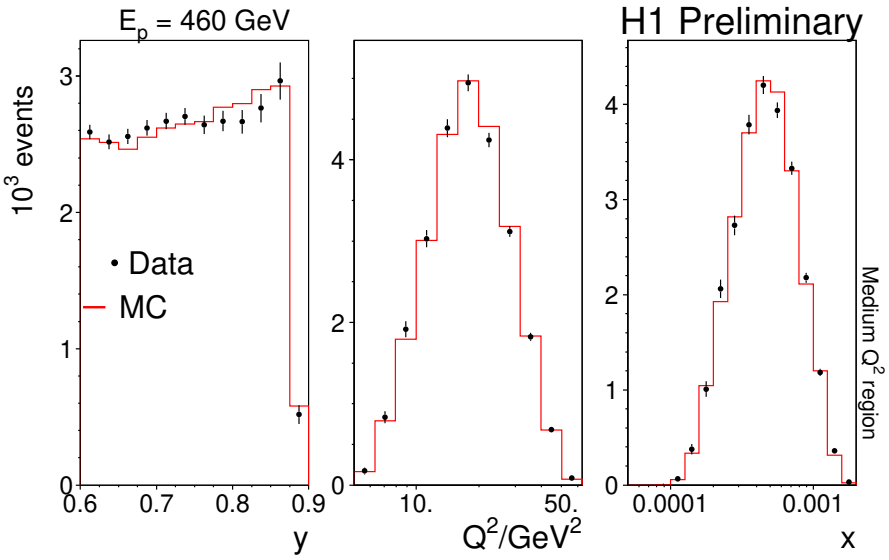

Figure 6: Comparison of signal distributions (background subtracted with corresponding asymmetry factor) for the low proton beam energy (460 GeV). The distributions from the left to the right are the inelasticity y, the four-momentum transfer squared Q^2 and Bjorken x.

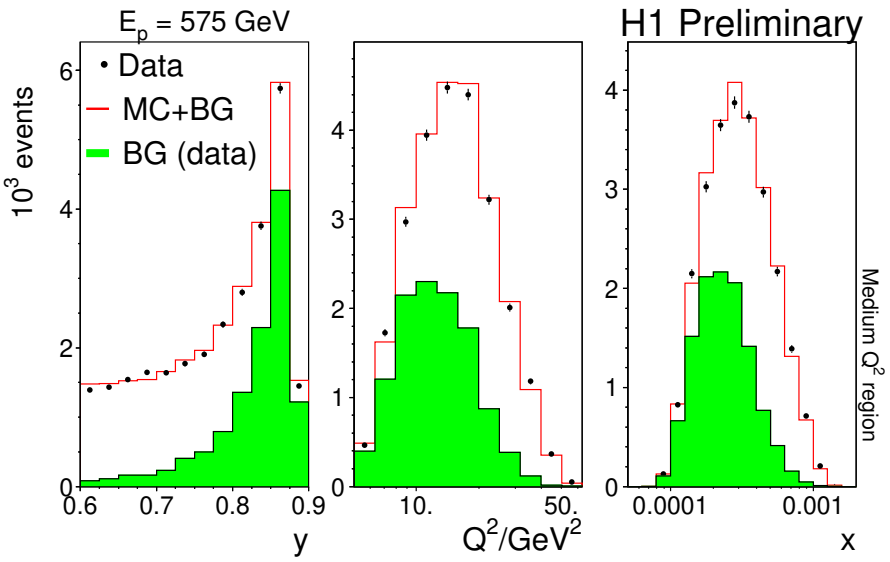

Figure 7: Comparison of the correct charge sign data (points) with a sum of background determined from the wrong charge sign data and DIS MC (open histogram) for the medium proton beam energy (575 GeV). The distributions from the left to the right are the inelasticity y, the four-momentum transfer squared Q^2 and the Bjorken x.

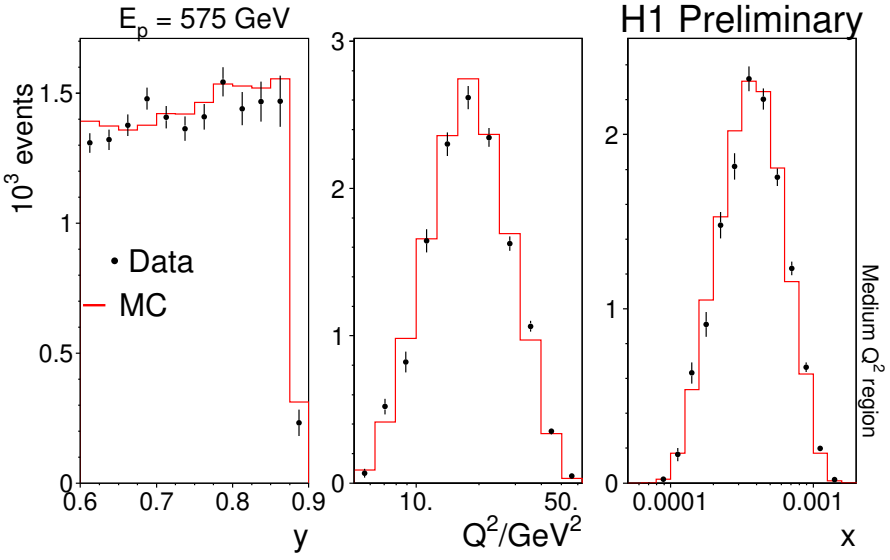

Figure 8: Comparison of signal distributions (background subtracted with corresponding asymmetry factor) for the the medium proton beam energy (575 GeV). The distributions from the left to the right are the inelasticity y, the four-momentum transfer squared Q^2 and the Bjorken x.

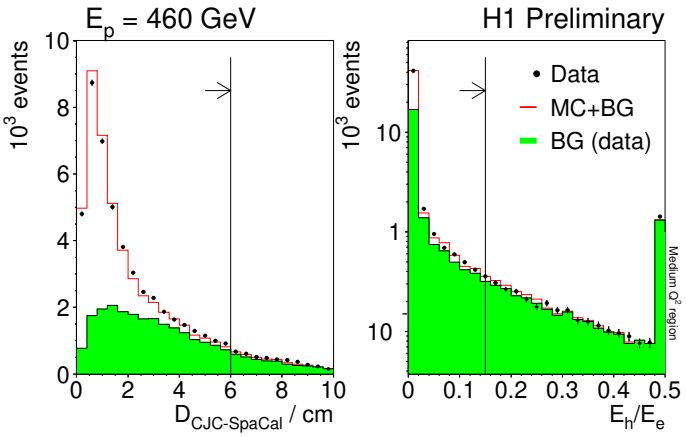

Figure 9: Comparison of the correct charge sign data (points) with a sum of background determined from the wrong charge sign data (green histogram) and DIS MC (open histogram) for the low proton beam energy (460 GeV). The distributions are distance between the extrapolated CJC track and cluster in SpaCal $D_{CJC-SpaCal}$ and fraction of the energy in the hadronic SpaCal behind the electromagnetic cluster E_h/E_e, respectively. The vertical lines in $D_{CJC-SpaCal}$ and E_h/E_e distributions indicate cut values.

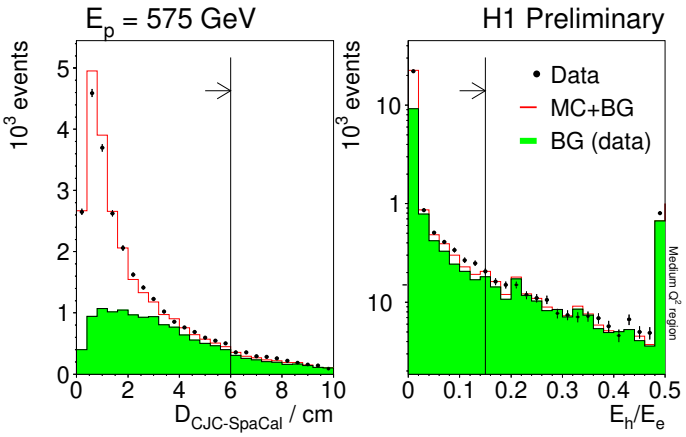

Figure 10: Comparison of the correct charge sign data (points) with a sum of background determined from the wrong charge sign data (green histogram) and DIS MC (open histogram) for the medium proton beam energy (575 GeV). The distributions are distance between the extrapolated CJC track and cluster in SpaCal $D_{CJC-SpaCal}$ and fraction of the energy in the hadronic SpaCal behind the electromagnetic cluster E_h/E_e, respectively. The vertical lines in $D_{CJC-SpaCal}$ and E_h/E_e distributions indicate cut values.

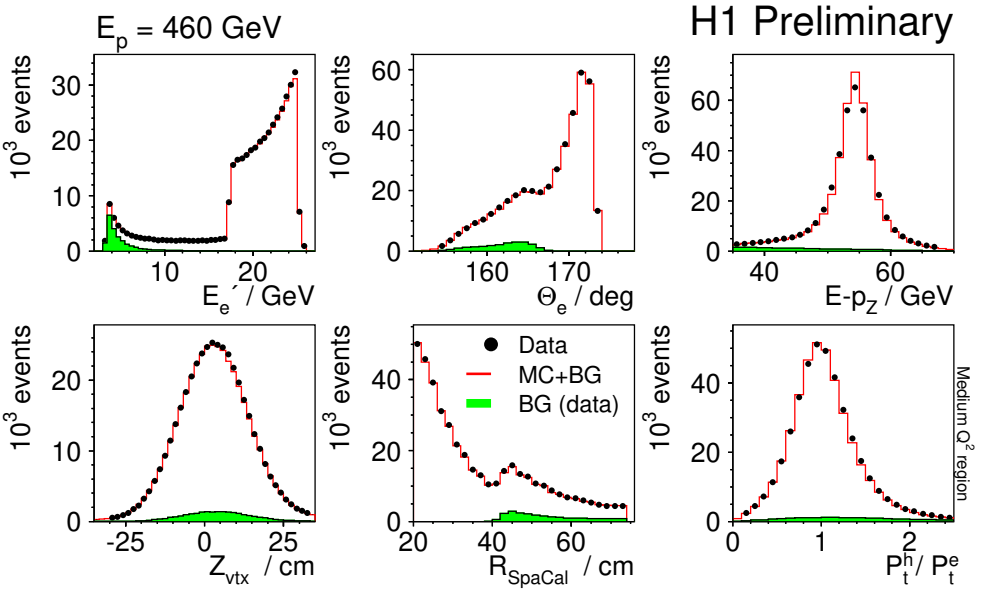

Figure 11: Comparison of the data (points) with a sum of background (green histogram) and DIS MC (open histogram) for the complete analysis range in y corresponding to the low proton beam energy (460 GeV). The distributions from the left to the right and from the top to the bottom are the scattered electron energy $E_e^{'}$, scattered electron polar angle Θ_e, the z-position of the event vertex Z_{vtx} and the sum $E - p_z$ of all final state particles, the logarithmic weighted cluster radius R_{SpaCal} and momentum balance P_t^h/P_t^e.

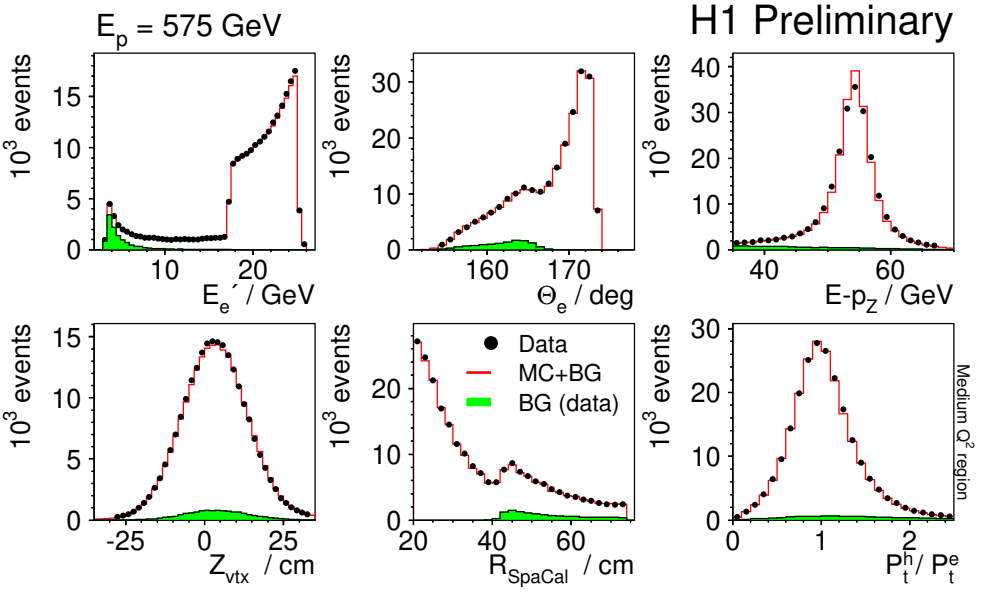

Figure 12: Comparison of data (points) with a sum of background determined from photoproduction MC (green histogram) and DIS MC (open histogram) for the complete analysis range in y corresponding to the medium proton beam enery (575 GeV). The distributions from the left to the right and from the top to the bottom are the scattered electron energy $E_e^{'}$, the scattered electron polar angle Θ_e, the z-position of the event vertex Z_{vtx} and the sum $E - p_z$ of all final state particles, the logarithmic weighted cluster radius R_{SpaCal} and the momentum balance P_t^h/P_t^e.

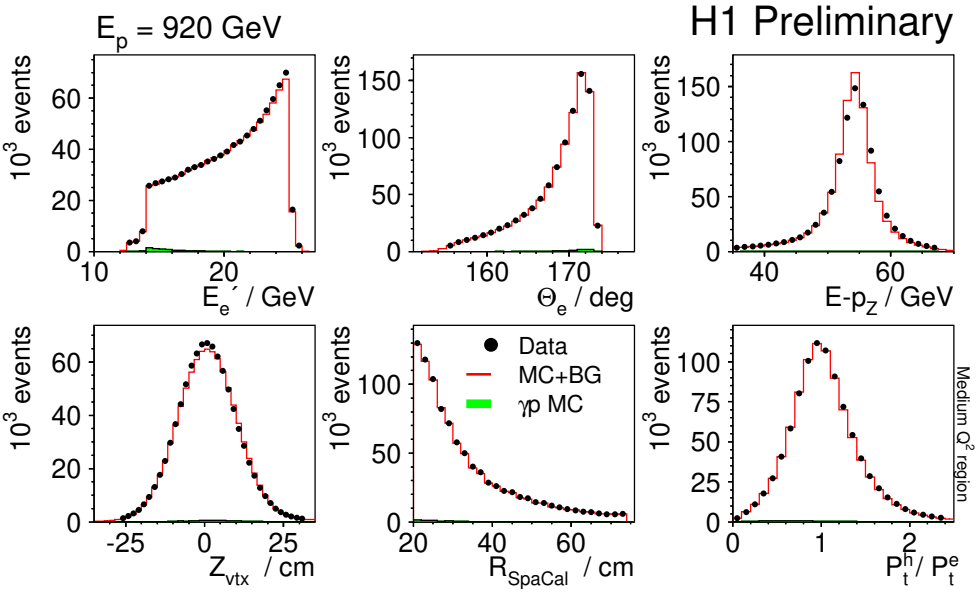

Figure 13: Comparison of the data (points) with a sum of background determined from photoproduction MC (green histogram) and DIS MC (open histogram) for the complete analysis range in y corresponding to the nominal proton beam energy (920 GeV). The distributions from the left to the right and from the top to the bottom are of the scattered electron energy E'_e, scattered electron polar angle Θ_e, the z-position of the event vertex Z_{vtx} and the sum $E - p_z$ of all final state particles, logarithmic weighted cluster radius R_{SpaCal} and the momentum balance P_t^h / P_t^e.

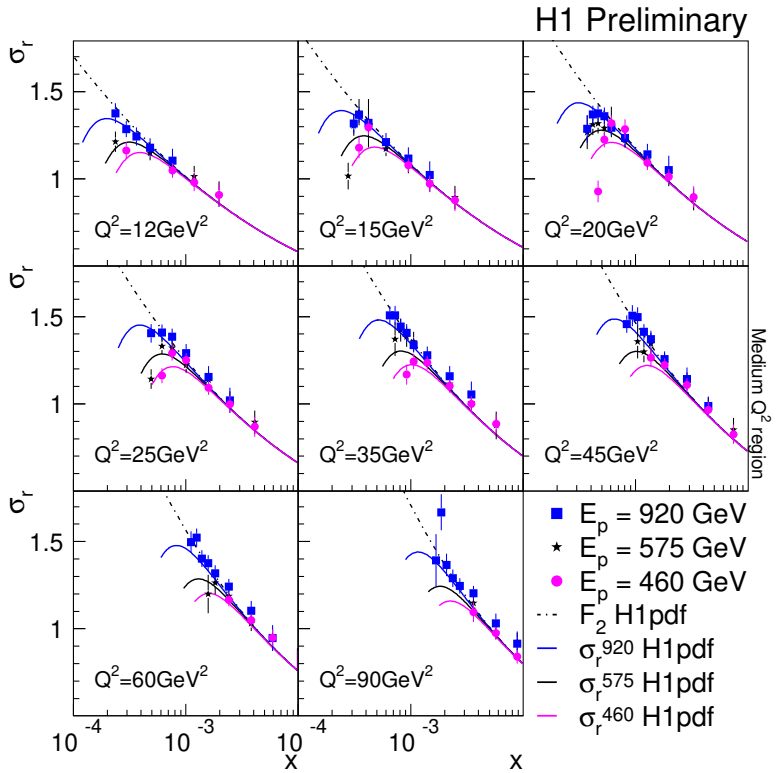

Figure 14: Reduced cross section measured at medium Q^2 as a function of x using data taken at different proton beam energies of 920 GeV (full boxes), 575 GeV (stars) and 460 GeV (full points). The error bars represent the statistical and systematic errors, added in quadrature. Theoretical predictions of reduced cross section are shown as the solid lines for 920 GeV (blue), 575 GeV (black) and 460 GeV (red) line. The dashed line represents the QCD expectation of F_2 derived from H1PDF fit.

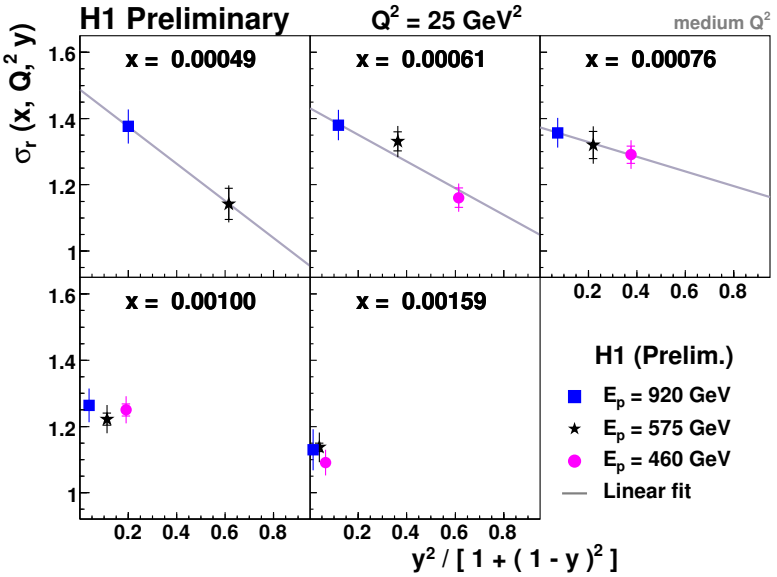

Figure 15: The reduced cross section $\sigma_r(x, Q^2, y)$ measured at $Q^2 = 25\ GeV^2$ and fixed values of x as a function of $f(y) = \frac{y^2}{1+(1-y)^2}$. The full boxes represent the nominal energy data (920 GeV), stars the medium energy data (575 GeV) and full circles the low energy data (460 GeV). The inner error bars are the statistical errors and the full error bars represent the statistical and systematic errors, added in quadrature. The lines show the linear fits used to determine F_L.

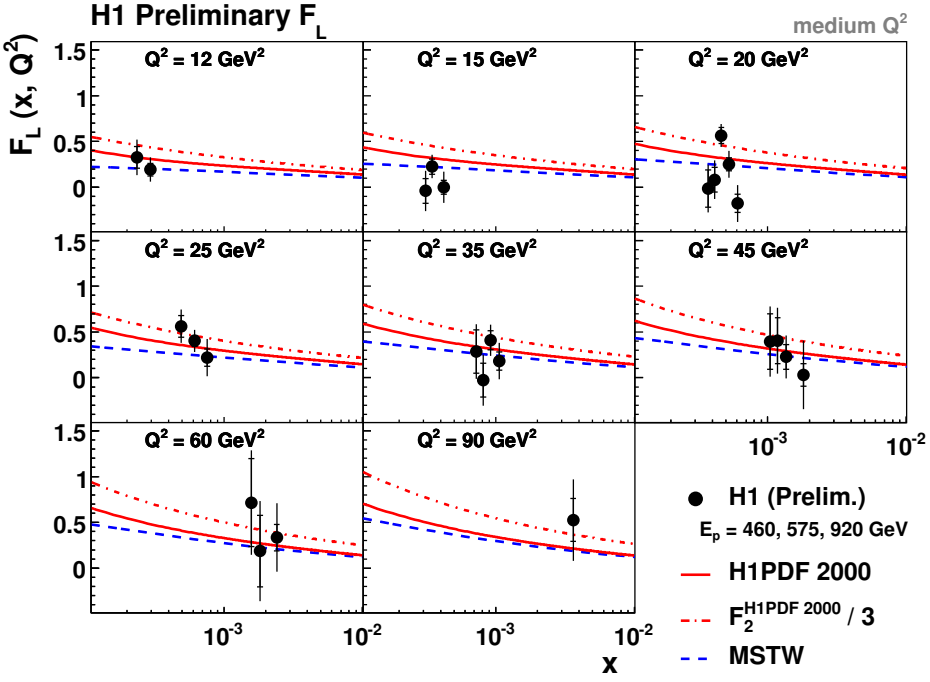

Figure 16: The longitudinal structure function F_L measured as a function of x at fixed values of Q^2 obtained by H1 using data taken at different proton beam energies of 460 GeV, 575 GeV and 920 GeV. The inner error bars are the statistical errors and the full error bars represent the statistical and systematic errors, added in quadrature. The solid red line represents a QCD prediction based on H1 PDF 2000 fit, the dashed red line $F_2^{H1PDF2000}/3$ and the dashed blue line a QCD prediction based on MSTW PDF.

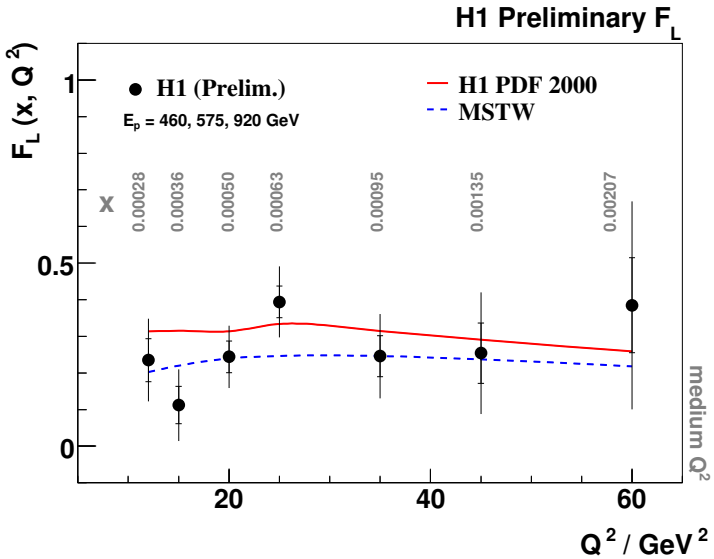

Figure 17: The longitudinal structure function $F_L(x, Q^2)$ averaged for a given Q^2 as measured by H1 using data taken at different proton beam energies of 460 GeV, 575 GeV and 920 GeV. The x values of the measurements contributing to the Q^2-value are indicated in grey. The inner error bars are the statistical errors and the full error bars represent the statistical and systematic errors, added in quadrature. The solid red line represents QCD prediction based on H1 PDF 2000 fit and the dashed blue line QCD prediction based on MSTW.

Systematic source	**Effect on the cross section**
Kinematic reconstruction	$\sim 3\%$
Electron identification and event selection	$\sim 2\%$
Background subtraction	max 4%
Radiative corrections	$\sim 1\%$

Table 1: Sources of systematic uncertainties and their impact on the cross section measurement.